PAPER Nr.: 28

FREE-WAKE ANALYSIS OF TWIN-ROTOR SYSTEMS

BY

J. GORDON LEISHMAN AND ASHISH BAGAI

CENTER FOR ROTORCRAFT EDUCATION AND RESEARCH
DEPARTMENT OF AEROSPACE ENGINEERING
UNIVERSITY OF MARYLAND AT COLLEGE PARK
MARYLAND 20742, USA

TWENTIETH EUROPEAN ROTORCRAFT FORUM
OCTOBER 4 - 7, 1994 AMSTERDAM

Printed by the Technical Highschool Haarlem

FREE-WAKE ANALYSIS OF TWIN-ROTOR SYSTEMS

J. Gordon Leishman* Ashish Bagai†

Center for Rotorcraft Education and Research,
Department of Aerospace Engineering,
University of Maryland at College Park, Maryland 20742, USA.

ABSTRACT - A free-wake analysis of twin-rotor systems is described. The analysis uses a recently developed pseudo-implicit predictor-corrector (PIPC) relaxation algorithm for the solution of the governing differential equations of the tip vortex geometries. Typical results are shown for tandem, side-by-side and co-axial rotor configurations.

NOMENCLATURE

c	Blade chord, m	C_T	Rotor thrust coefficient, $T/\rho\pi R^2(\Omega R)^2$
C_Q	Rotor torque coefficient, $Q/\rho\pi R^2(\Omega R)^2 R$	$\hat{i}$, $\hat{j}$, $\hat{k}$	Unit vectors in the x, y and z directions, respectively
N_b	Number of blades	N_v	Number of vortex filaments
Q	Rotor torque, Nm	$\vec{r}$	Position of a point on a wake filament, m
r_c	Vortex core radius, m	r_v	Radial position from which wake
	filaments are trailed, m	R	Rotor radius, m
T	Rotor thrust, N	v_θ	Tangential velocity, m/s
V_∞	Free–stream velocity, m/s	$\vec{V}_{ind}$	Induced velocity, m/s
x, y, z	Cartesian coordinate system, origin at hub center of rotor 1, m	α_s	Rotor shaft angle, deg.
β_0	Blade coning angle, deg.	Γ	Circulation, m^2/s
λ_i	Uniform induced inflow ratio	μ	Rotor advance ratio, $V_\infty/\Omega R$
Ω	Rotational frequency of rotor, rad/s	ψ	Azimuth angle, rad.
$\chi_{...}$	Position of rotor hub 2 relative to hub 1, m	ζ	Distance along trailed wake filament, rad

1. INTRODUCTION

The improved modeling of a helicopter rotor flow field remains fundamental to enhanced predictions of rotor loads, performance, and acoustics. It has been documented experimentally that a helicopter rotor wake is dominated by strong vortices that quickly form behind each blade tip, see for example, Refs. 1 and 2. The strengths and initial positions of these tip vortices are related to the individual blade lift distributions. As each blade rotates, the tip vortices are left in space behind the rotor, and are convected to new positions by the influence of the local induced velocity field. Unlike a fixed-wing aircraft, rotor tip vortices remain relatively close to the rotor, and have a powerful influence on the distribution of aerodynamic loading on each blade. Large temporal variations in local blade loading may also result, leading to impulsive noise generation from the rotor.

The wake geometry emanating from a single rotor is known to be affected by many interrelated geometric parameters (such as blade twist, planform, and number of blades) and operational

*Associate Professor.

†Graduate Research Assistant.

Presented as paper No. 28, 20^{th} European Rotorcraft Forum, Amsterdam, The Netherlands, 4-7 October 1994.

conditions (such as rotor thrust, advance ratio, climb velocity, and tip path plane angle of attack). Rotor/airframe interference effects are also known to have an important effect on the wake geometry.[3, 4] For multi-rotor systems, the problem becomes considerably more complicated, mostly because the interference between each rotor results in considerable mutual distortion of each wake system. In addition, there is an increased likelihood of blade vortex interactions or BVI for multi-rotor systems, particularly since the wake from one rotor can often be ingested directly into the other. BVI is known to be a particularly dominant source of noise for tandem rotor configurations.[5, 6] With the more stringent civil and military noise standards, minimizing noise generation from both single and multi-rotor systems will become an increasingly important factor in the rotor design process.

The mathematical modeling of either single or multi-rotor wake systems at any realistic level of sophistication is, unfortunately, a problem of formidable complexity. Modern comprehensive rotor codes typically include sophisticated structural and dynamic models of the rotor system, yet the aerodynamic model is usually less sophisticated. This is at least in part because of the large computational resources required for realistic aerodynamic models of the rotor wake system and the corresponding induced velocity field. Existing wake models used in modern comprehensive rotor analyses range from fairly simple "prescribed" or semi-empirical wakes to more sophisticated "free" wakes. Refs. 7-11 describe typical prescribed wake models for single rotors where the rotor tip vortex trajectories are described by functional modifications to the classical or "rigid" cycloidal wake. The velocity field induced by the rotor wake is then calculated by the application of the Biot–Savart law integrated along the prescribed trajectory of each tip vortex filament. Wake distortion functions, specified empirically in terms of rotor geometric and operational factors, are used to distort the wake with the aid of wake geometry measurements from small scale rotors.[12, 13] Although computationally efficient and of considerable use in routine rotor design work, prescribed wake models do not fully capture the physical nature of the wake. Furthermore, since these models are constructed based on a limited number of rotor experiments, their applicability to more general rotor configurations is questionable. Nevertheless, because of their computational efficiency, prescribed wake models have been widely used for both single[7, 10, 11] and co-axial rotor configurations.[14, 15]

The next level of sophistication in rotor wake modeling is the so-called "free" wake analysis. Free-wake models solve for the wake directly and, at least in principle, do not require experimentally obtained wake geometry data for formulation purposes. However, since both the positions and the strengths of the individual wake filaments are now part of the solution process, free-wake models are obviously much more computationally intensive. Pioneering work on the free-wake solution methodology for single rotors was performed about 20-years ago by Clark and Leiper[16] and Sadler,[17] and many variations and developments of the basic approach have subsequently followed. In the most basic free-wake methodology, an explicit-type algorithm is used to extrapolate the wake geometry to a force-free position.* However, one of the well known problems of these schemes is their susceptibility to numerical instabilities. One solution is to implement improved integration schemes, and while several such implementations are possible, this is usually at the expense of significantly increasing the overall computational expense. For example, Miller and Bliss[18] showed that by using a semi-implicit formulation for the free-wake solution, many of the numerical problems that have been characteristic of explicit models could be avoided, however, implicit schemes require the inversion of large matrices per iteration/time step, making them computationally very expensive for use in comprehensive rotor codes. Also, it has been demonstrated in Ref. 18 that even semi-implicit methods do not necessarily converge to a steady-state solution, especially in hover or at low advance ratios.

More recently, Bagai and Leishman[19, 20] showed that a pseudo-implicit predictor-corrector (PIPC) method with spatial averaging can be used to stabilize the numerical computation of the free-wake, without the use of artificial damping. Because of improved convergence relative to the explicit scheme, the overall computational expense with the PIPC scheme can be significantly reduced. Such an approach draws a good compromise between minimizing numerical errors and helping to maximize computational efficiency. Excellent wake convergence characteristics for single rotors operating in hover and low speed forward flight have been demonstrated with the PIPC method, and the predictions have also shown good agreement with experimental data for single rotors. In this paper, we extend this work and examine some of the special problems in predicting the wakes of twin-rotor systems including co-axial, tandem and side-by-side configurations.

*Explicit algorithms are used in several well known comprehensive helicopter rotor codes.

2. METHODOLOGY

In the present analysis, each rotor blade is assumed to trail a concentrated vortex from the vicinity of the rotor blade tip. The blade itself is modeled as a lifting surface (Weissinger L-model) with an unsteady near wake model for trailed and shed vorticity immediately behind each blade. The near wake model defines the initial strengths and locations of the rolled-up blade tip vortices, and is treated as a boundary condition for the free-wake problem. The strength and location of the tip vortex relative to the blade at any given azimuth position (time) is determined by the spanwise lift distribution over each blade. While the roll-up of the wake is known to be a physically complex process, it is known from experiments that rotors develop single concentrated tip vortices (at least with blades that have conventional tip shapes) that form almost immediately behind the blade. In the present work, the tip vortex strength and position is computed based on a variation of Rossow's centroid of vorticity approach.[21]

A numerical solution to the subsequent positions of the tip vortices that are trailed from each blade can be obtained by the integration of a system of ordinary differential equations (ODE's). These ODE's are obtained by the spatial discretization of the partial differential equations (PDE's) that govern the actual convection of the vortex filaments to force-free positions. As described in Ref. 19, the governing PDE for a typical tip vortex filament can be written as

$$\frac{\partial \vec{r}(\psi,\zeta)}{\partial \psi} + \frac{\partial \vec{r}(\psi,\zeta)}{\partial \zeta} = \frac{\vec{V}_\infty}{\Omega} + \frac{1}{\Omega}\sum_{i=1}^{N_v} \vec{V}_{ind}(\vec{r}(\psi,\zeta),\vec{r}(\psi_i,\zeta)) \tag{1}$$

where the V_{ind} term on the right-hand-side collectively represents the velocities induced by all the free or bound vortices in the flow field.

Induced Velocities

The source terms due to the wake are obtained by integrating over all the trailed vortex filaments by means of the Biot–Savart law. Obviously, if a potential vortex is used in this process then the induced velocity becomes singular when wake collocation points approach the axis of any vortex filament. Obviously, this may result in numerical problems, but can be alleviated by using a viscous vortex model with a finite core radius. In Ref. 22, it was shown that the tangential velocity profile of rotor tip vortices can be closely approximated by

$$v_\theta(r) = \frac{\Gamma r}{2\pi\sqrt{{r_c}^4 + r^4}} \tag{2}$$

where r_c is the initial viscous core radius.† The effects of diffusion can be incorporated with a slight modification the Biot-Savart law

$$\vec{V}_{ind}(\vec{r}(\psi,\zeta),\vec{r}(\psi_j,\zeta)) \equiv \frac{\Upsilon}{4\,\pi}\int \frac{\Gamma(\psi_j,\zeta)\; d\vec{\zeta_j} \times (\vec{r}(\psi,\zeta) - \vec{r}(\psi_j,\zeta))}{\mid \vec{r}(\psi,\zeta) - \vec{r}(\psi_j,\zeta) \mid^3} \tag{3}$$

where $\vec{r}\,(\psi,\zeta)$ is the point in the flow field influenced by the i^{th} vortex at location $\vec{r}\,(\psi_i,\zeta)$ and of strength (circulation) $\Gamma(\psi_i,\zeta)$. The parameter Υ is given in terms of geometric and aerodynamic parameters by

$$1 - \exp\left(\frac{-AR\;Re\;\bar{r}^2}{4\pi\zeta\;\delta}\right) \tag{4}$$

where $\bar{r} = r/R$, AR is the rotor blade aspect ratio, and Re is the Reynolds number in terms of tip speed and blade chord. The factor δ is a viscous decay factor that must be selected empirically – see, for example, Lamb.[23] For a laminar vortex, δ=1 and the diffusion is extremely slow since it is governed only by the kinematic viscosity of the fluid. However, various workers have shown that it is

†Physically, the initial tip vortex core radius on helicopter rotors is known to be of the order of blade thickness (typically 10-15% of mean blade chord).

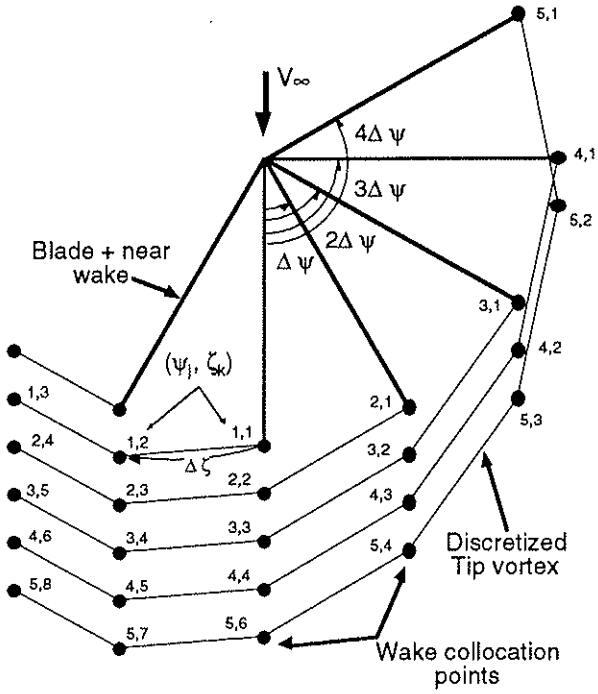

Figure 1: Discretized physical domain for free-wake of typical tip vortex

possible to allow for an "eddy" viscosity due to the degree of turbulence adjusting the value of δ by comparisons of calculation with experiment. From the work in Ref. 20, it is known that δ is of order of magnitude 10^4 for single rotors, and this value has been retained for all the calculations reported in this article.

The wake induced velocities are largely responsible for the highly nonlinear space and time-dependent forcing or *source* terms that describe the physical distortion and roll-up of the rotor wake. Note that the effect of the eddy viscosity coefficient, δ, is to gradually diffuse the vorticity radially outward as a function of wake age, that is the age of a filament relative to the blade from which it originated. Depending on the value chosen for δ, the wake may relax to a physically correct solution, or may over- or under-relax to non-physical solutions. Such issues are discussed in Ref. 20

In addition to the physics of diffusion covered by Eq. 4, the possibility of vorticity intensification due to straining of the vortex filaments must be considered. In some locations, particularly in regions where the tip vortex filaments "pair" and roll-up into bundles, considerable straining is possible. This may be an especially important problem for multi-rotor systems where there are typically many vortex filaments, and the probability of vortex/vortex distortions is relatively high. While an exact treatment of this problem is obviously impractical within the scope of the present model, a representation of the basic effect can be made using a simpler approach where the vorticity is assumed to lie entirely within the vortex core, r_c (which is the case strictly only for a Rankine vortex). The application of conservation of mass and angular momentum then leads to a simple relationship between the filament strain and the change in the local core size – see Ref. 20.

Free-Wake Scheme

If a series of collocation points are specified along the lengths of the trailed vortex filaments generated by each blade, these points must then be continuously convected through the flow field at the local velocity. The discretized physical domain for one rotor blade is shown in Fig. 1. Note that in this discretized representation, there is one equation such as Eq. 1 for every point in the wake. Clearly, the number of subdivided wake segments determine the far wake resolution, but also increase the computational size of the numerical problem. One must often, therefore, make a compromise between resolution versus computational cost for the free-wake model.

For the numerical solution of the wake equations, Eq. 1 must first be cast into finite-difference form. In the present work, a five-point central difference approximation is used, where the derivatives

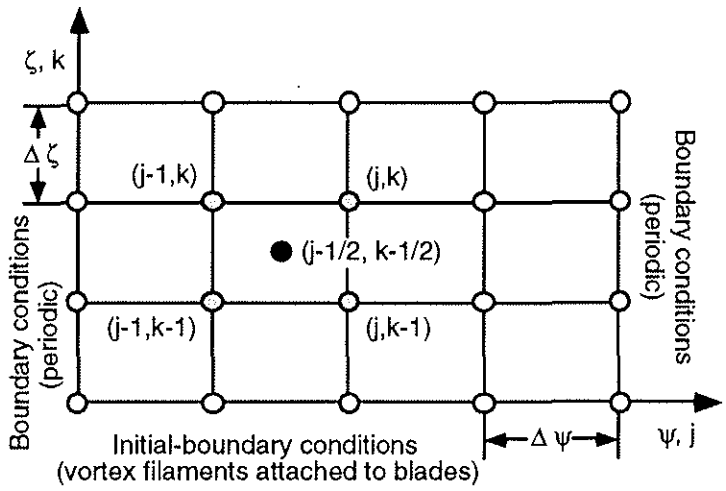

Figure 2: Discretized computational domain for governing PDE

on the left-hand side are evaluated at point $(k-\frac{1}{2}, i-\frac{1}{2})$ about points (k,i), $(k,i-1)$, $(k-1,i)$ and $(k-1,i-1)$, see Fig. 2. The next step is to advance the solution to obtain force-free positions for the vortex filaments. In a typical explicit scheme, the current solution is obtained by extrapolating from the previous iteration over a finite "time" increment, $\Delta\psi$, by means of a single, backward finite difference step, i.e., $\vec{r}^{\,n}_{j,k} = f(\vec{r}^{\,n-1}_{j-1,k-1}, \vec{r}^{\,n-1}_{j-1,k}, \vec{r}^{\,n-1}_{j,k-1})$ and $\vec{V}_{ind} = g(\vec{r}^{\,n-1}_{j-1,k-1}, \vec{r}^{\,n-1}_{j-1,k}, \vec{r}^{\,n-1}_{j,k-1})$. Although this may be one of the simplest methods to implement, it is only first order accurate and the accumulation of discretization errors over a number of iterations often results in the method becoming numerically unstable. Therefore, such methods normally require the inclusion of some form of artificial damping. Unfortunately, for rotor free-wake problems which are highly nonlinear, the damping is a function of the flight condition (i.e., thrust and advance ratio) and is not known *à priori*.

Various improvements in the accuracy and stability of explicit schemes may be made by using a predictor-corrector methodology, and usually without the need for artificial numerical damping. However, predictor-corrector (PC) schemes require two velocity field calculations per time step compared to the explicit method. In the PC approach, the corrected solution at the current n^{th} iteration is obtained by averaging the induced velocity from the previous $(n-1)^{th}$ iteration with the predicted induced velocities from the current n^{th} iteration predictor step. The enhanced stability and increased convergence rates of such schemes normally out-weigh the additional computational expense of performing two induced velocity calculations per iteration. PC methods are known to be almost universally advantageous where the function evaluation on the right-hand-side of the equations is computationally expensive.[24]

A further improvement to the basic PC scheme has been discussed in Ref. 20 resulting in a *pseudo-implicit* (PIPC) scheme for both the predictor and corrector steps. These equations can be written as

Predictor:

$$\begin{aligned}
\tilde{\vec{r}}^{\,n}_{j,k} &= \tilde{\vec{r}}^{\,n}_{j-1,k-1} + \left(\frac{\Delta\psi-\Delta\zeta}{\Delta\psi+\Delta\zeta}\right)\left(\tilde{\vec{r}}^{\,n}_{j,k-1} - \tilde{\vec{r}}^{\,n}_{j-1,k}\right) \\
&+ \left(\frac{\Delta\psi\Delta\zeta}{\Delta\psi+\Delta\zeta}\right)\frac{2}{\Omega}\left(\vec{V}_\infty + \frac{1}{4}\left(\sum_{i=1}^{N_v}\vec{V}_{ind}(\vec{r}^{\,n-1}_{j-1,k-1}, \vec{r}^{\,n-1}_{i,\zeta}) + \sum_{i=1}^{N_v}\vec{V}_{ind}(\vec{r}^{\,n-1}_{j-1,k}, \vec{r}^{\,n-1}_{i,\zeta})\right.\right. \\
&+ \left.\left.\sum_{i=1}^{N_v}\vec{V}_{ind}(\vec{r}^{\,n-1}_{j,k-1}, \vec{r}^{\,n-1}_{i,\zeta}) + \sum_{i=1}^{N_v}\vec{V}_{ind}(\vec{r}^{\,n-1}_{j,k}, \vec{r}^{\,n-1}_{i,\zeta})\right)\right)
\end{aligned} \tag{5}$$

Corrector:

$$\vec{r}^{\,n}_{j,k} = \vec{r}^{\,n}_{j-1,k-1} + \left(\frac{\Delta\psi-\Delta\zeta}{\Delta\psi+\Delta\zeta}\right)\left(\vec{r}^{\,n}_{j,k-1} - \vec{r}^{\,n}_{j-1,k}\right)$$

$$+ \quad \left(\frac{\Delta\psi\Delta\zeta}{\Delta\psi+\Delta\zeta}\right)\frac{2}{\Omega}\left(\vec{V}_\infty+\frac{1}{4}\left(\sum_{i=1}^{N_v}\overline{\vec{V}}_{ind}(\vec{r}_{j-1,k-1},\vec{r}_{i,\zeta})+\sum_{i=1}^{N_v}\overline{\vec{V}}_{ind}(\vec{r}_{j-1,k},\vec{r}_{i,\zeta})\right.\right.$$
$$\left.\left.+\quad\sum_{i=1}^{N_v}\overline{\vec{V}}_{ind}(\vec{r}_{j,k-1},\vec{r}_{i,\zeta})+\sum_{i=1}^{N_v}\overline{\vec{V}}_{ind}(\vec{r}_{j,k},\vec{r}_{i,\zeta})\right)\right) \tag{6}$$

where the induced velocity vectors, $\overline{\vec{V}}_{ind}(\cdots,\cdots)$, are defined by

$$\begin{aligned}
\overline{\vec{V}}_{ind}(\vec{r}_{j-1,k-1},\vec{r}^{\,n-1}_{i,\zeta}) &= \frac{1}{2}\left(\vec{V}_{ind}(\vec{r}^{\,n-1}_{j-1,k-1},\vec{r}^{\,n-1}_{i,\zeta})+\vec{V}_{ind}(\tilde{\vec{r}}^{\,n}_{j-1,k-1},\tilde{\vec{r}}^{\,n}_{i,\zeta})\right)\\
\overline{\vec{V}}_{ind}(\vec{r}_{j-1,k},\vec{r}^{\,n-1}_{i,\zeta}) &= \frac{1}{2}\left(\vec{V}_{ind}(\vec{r}^{\,n-1}_{j-1,k},\vec{r}^{\,n-1}_{i,\zeta})+\vec{V}_{ind}(\tilde{\vec{r}}^{\,n}_{j-1,k},\tilde{\vec{r}}^{\,n}_{i,\zeta})\right)\\
\overline{\vec{V}}_{ind}(\vec{r}_{j,k-1},\vec{r}_{i,\zeta}) &= \frac{1}{2}\left(\vec{V}_{ind}(\vec{r}^{\,n-1}_{j,k-1},\vec{r}^{\,n-1}_{i,\zeta})+\vec{V}_{ind}(\tilde{\vec{r}}^{\,n}_{j,k-1},\tilde{\vec{r}}^{\,n}_{i,\zeta})\right)
\end{aligned}$$

Note that the source terms (which are comprised of the induced velocities on the right-hand-side of Eqs. 5 and 6) are still treated explicitly, in that the final values for the induced velocities are computed using averages of the previous iteration and the predicted values from the current iteration. The position vectors, $\tilde{\vec{r}}^{\,n}_{\cdots,\cdots}$ are predicted values returned by the explicit predictor step given by Eq. 5. This scheme has a truncation error of $\mathcal{O}^3$ per step and better stability characteristics than fully explicit predictor–corrector methods alone.

Boundary Conditions

Since the PDE governing the free-wake problem is first order in ψ and ζ, the solution of the problem requires the specification of two initial/boundary conditions, one in the ψ direction, and one in the ζ direction.[‡] First, to give the "initial"-boundary condition in the ζ direction for each ψ, the trailed vortex elements are attached to the blades (or in the present case, to the near wake). Second, wake periodicity is enforced as the boundary condition in the ψ direction – see Fig. 2. The solution is subsequently stepped in the ζ direction in an iterative manner, and convergence is obtained once the wake geometry no longer distorts within a prescribed tolerance between successive iterations.

Mathematically, the boundary and initial conditions for any rotor blade may be stated as

Boundary conditions:

$$\vec{r}(\psi,\zeta)=\vec{r}(\psi+2\pi,\zeta) \tag{7}$$

Initial-Boundary conditions: ($\zeta=0$)

$$\begin{aligned}
\vec{r}(\psi,\zeta) &= r_v(\cos(\beta_0)\cos(\psi)\cos(\alpha_s)+\sin(\beta_0)\sin(\alpha_s))\,\hat{i}\\
&+ \quad r_v\cos(\beta_0)\sin(\psi)\,\hat{j}\\
&+ \quad r_v(\sin(\beta_0\cos(\alpha_s)-\cos(\beta_0)\cos(\psi)\sin(\alpha_s)\,\hat{k}
\end{aligned} \tag{8}$$

It will be recognized that the free wake analysis of a twin rotor system is considerably more complex than that for a single rotor configuration due to the presence of two mutually interacting rotor wakes. As for the single rotor case, the solution of the twin rotor problem requires the specification of two initial/boundary conditions per rotor. While each rotors wake is specified to be attached to

[‡]Note that while ζ is a spatial coordinate, ψ can be interpreted as either a temporal coordinate (as would be the case for a time-stepping wake scheme), or as a spatial coordinate (as used here) when incorporating a relaxation methodology.

its near wake as the "initial-boundary" condition in the ζ direction, and wake periodicity enforced in the ψ direction, the initial starting induced velocity field is calculated based on a prescribed wake geometry for each rotor. In the present case, a classical undistorted wake has been used, which is given by

$$\begin{aligned}
\vec{r}(\psi,\zeta) &= (\chi_x + r_v(\cos(\beta_0)\cos(\pm\psi \mp \zeta)\cos(\alpha_s) + \sin(\beta_0)\sin(\alpha_s) \\
&- \lambda_i(\cos(\alpha_s)\cos(\pm\psi \mp \zeta)\sin(\beta_0) + \sin(\alpha_s)\cos(\beta_0)) + \mu\zeta))\hat{i} \\
&+ (\chi_y + r_v(\cos(\beta_0)\sin(\pm\psi \mp \zeta) + \lambda_i \sin(\pm\psi \mp \zeta)\sin(\beta_0)))\hat{j} \\
&+ (\chi_z + r_v(\sin(\beta_0)\cos(\alpha_s) - \cos(\beta_0)\cos(\pm\psi \mp \zeta)\sin(\alpha_s) \\
&- \lambda_i(\sin(\alpha_s)\cos(\pm\psi \mp \zeta)\sin(\beta_0) + \cos(\alpha_s)\cos(\beta_0))\zeta))\hat{k} \qquad (9)
\end{aligned}$$

Note that blade azimuth and wake collocation point angles are positive for a counter-clockwise rotating rotor and negative for a rotor turning in the clockwise direction. Furthermore, note also that the origin of the fixed frame Cartesian coordinate system is located at the hub of the first (reference) rotor (R-1) and that χ_x, χ_y and χ_z represent the (x, y, z) displacements of the second rotor (R-2) hub relative to the first rotor hub. That is, $\chi_x = 0$, $\chi_y = 0$ and $\chi_z = 0$ for R-1, where as one or all of the quantities are specified for R-2. Remember that this initial prescribed wake geometry is used only to provide an approximate induced velocity field to start the free-wake calculations. In practice, it has been found that because wake convergence is so rapid with the PIPC scheme, the convergence rate and final solution is insensitive to these initial starting conditions. For the twin rotor system however, the mutual interactions of the tip vortices from both rotors result in significant mutual interactions, and for such cases, a fairly accurate initial starting condition can help enhance wake convergence trends.

Twin Free-Wake Implementation

As mentioned previously, in the present analysis the free wake equations have been solved using a pseudo-implicit relaxation methodology. For the twin rotor configuration, the total self- and mutual-induced velocity field due to the tip vortices from both rotors is calculated at each collocation point of the wake from R-1 using Eq. 3. The wake geometry for R-1 is then updated using the PIPC scheme and the process repeated for the wake from R-2. Thus, we have a situation where the update to the wake geometry from R-2 lags the wake from R-1 at every iteration. This sequential calculation, therefore, results in final wake geometries that are very slightly dissimilar for symmetric (such as side-by-side rotor) configurations. Nevertheless, the current pseudo-implicit method has been found to result in converged wake geometries for both rotors, even at advance ratios as low as μ=0.05.

Note that while the above issue could be resolved by first calculating the induced velocity fields on both rotor wakes before updating the wake geometries, the computational scheme would become unnecessarily complicated and would require about four times the storage of the present implementation. Since the whole objective is to integrate this free-wake analysis into a comprehensive rotor code, the extra storage expense is prohibitive in most cases.

Rotor Trim Methodology

The solution of the free-wake problem gives the aerodynamic velocity environment at the blade, and, therefore, the blade and rotor forces can be obtained by integration along the blade and around the azimuth. However, a helicopter rotor is also a dynamic system with some form of articulation allowing flapping, lead-lag and feathering (pitch) degrees-of-freedom. To make the computed results physically meaningful, the rotor blades must be allowed to flap under the action of the aerodynamic forces and moments on each blade so that the rotor reaches an equilibrium position. This equilibrium also depends on the geometric and inertial characteristics of the rotor blades, and can be controlled by the action of control inputs to give an appropriate trim state.

Obviously, a trimmed solution is essential when making comparisons with experimental data. However, the trim model for a rotor requires the solution of several coupled nonlinear equations involving rotor forces and moments. In the present analysis, a modified Newton-Raphson scheme with

a finite-difference approximation to the trim Jacobian was used to solve the trim equations at each free-wake iteration. Since each rotor was trimmed in thrust, longitudinal and lateral flapping via three control inputs, and the blade load calculations coupled to the wake from both rotors, the resulting Jacobian was 6 × 6 in dimension. For the co-axial and tandem configurations, a differential thrust requirement on the two rotors was specified so as to result in a specified net thrust, while maintaining approximately equal torque levels on both rotors, i.e. $C_{T_1} + C_{T_2} = C_{T_{total}}$ and $C_{Q_1} \equiv C_{Q_2}$. For the side-by-side configuration on the other hand, the thrust and torque coefficients on both rotors were the same due to the symmetry of the rotor configuration.

The rotor trim routine was called at every iteration to ensure that the final solution for the wake geometry was fully compatible with the specified trim state. Each rotor was trimmed independently to the specified thrust levels and zero first harmonic flapping with approximately equal torque coefficients. For twin rotor configurations, it is important that both rotors absorb the same amount of power such that zero yawing moments result, since unlike single rotor helicopters, there is no independent anti-torque (tail) rotor. Elimination of first harmonic flapping essentially results in the tip path planes of both rotors being perpendicular to the rotor shaft. While this has been obtained here through the application of independent lateral and cyclic controls to each rotor, actual tandem rotors have only collective and lateral cyclic on each rotor and differential collective. It is important to remember, therefore, that the present trim state corresponds to a wind-tunnel trim and not a propulsive (or free-flight) trim condition. Note however, that the trim methodology does account for the mutual aerodynamic interference effects of one rotor and its wake on the other.

3. RESULTS AND DISCUSSION

The robust nature of the present PIPC scheme has already been demonstrated for single rotor wakes.[19, 20] In Ref. 19 the scheme was compared to typical explicit methodologies and also validated by comparisons with experimental wake geometry results. Lateral and longitudinal inflow distributions over the rotor disk, and induced velocity field calculations downstream of the rotor also showed good correlation with measured data. Additional numerical aspects, such as the effect of spatial and temporal resolution of the wake, number of wake turns, initial vortex core radii etc. on the stability and convergence of the numerical scheme have been discussed in further detail in Ref. 20, as was the pseudo-implicitness of the method. Here we present some free-wake geometry results pertaining to the three basic representative twin rotor configurations, namely side-by-side, tandem and coaxial systems. Although numerous combinations of rotor separations and degrees of overlap are possible, it is naturally not possible to address all these issues in a single paper. Nevertheless, the configurations discussed here have been chosen based on two factors: First, that they be representative of currently flying models; and second, they represent the most challenging configurations from the numerical stand point. All results have been calculated for a moderate total system thrust coefficient, $C_{T_{total}}$=0.01 and at three advance ratios, μ=0.05, 0.075 and 0.1. Once again, these conditions represent the most difficult situations since the mutual interactions and distortions between the wake vortices are most severe under low speed flight conditions.

Typical top and rear converged wake geometries for the three rotor configurations are shown in Figs. 3 through 6 for an advance ratio of 0.05. Each rotor has three blades, and the rotors rotate in opposite directions. The co-axial rotor hubs are separated vertically by $0.2R$, the tandem rotors are also separated vertically by $0.2R$ and in the longitudinal direction by $1.3R$ allowing for 70%overlap. The side-by-side rotor hubs are separated laterally by $2.5R$ and lie in the same vertical plane. All rotor shafts have a forward tilt of 3 deg.

For the co-axial and tandem configurations, it can be seen from Fig. 3 that the wake structures for the two rotors are vastly different. For the co-axial rotor case, Fig. 3(a) and Fig. 4, the wake from the upper rotor quickly contracts as it is ingested into the streamtube of the lower rotor. The axial distortions to the tip vortices by way of stretching or elongation also appear to be much more severe. By the same count, this inner vortex tube tends to compress the outer vortex spirals from the lower rotor as compared to the single isolated rotors wake. It is interesting to note however, that the two rotor wakes do not appear to intertwine or coalesce into combined vortex bundles (this is true even at higher advance ratios) but retain their individual concentric structures. This is confirmed by the experimental observations of co-axial wakes in Ref. 25. In addition, the free wake calculations have been run for a finite number (three turns) of vortex filament lengths. The second (upper) rotor wake therefore, is pulled through and exits the outer (lower rotors) streamtube, expanding out from

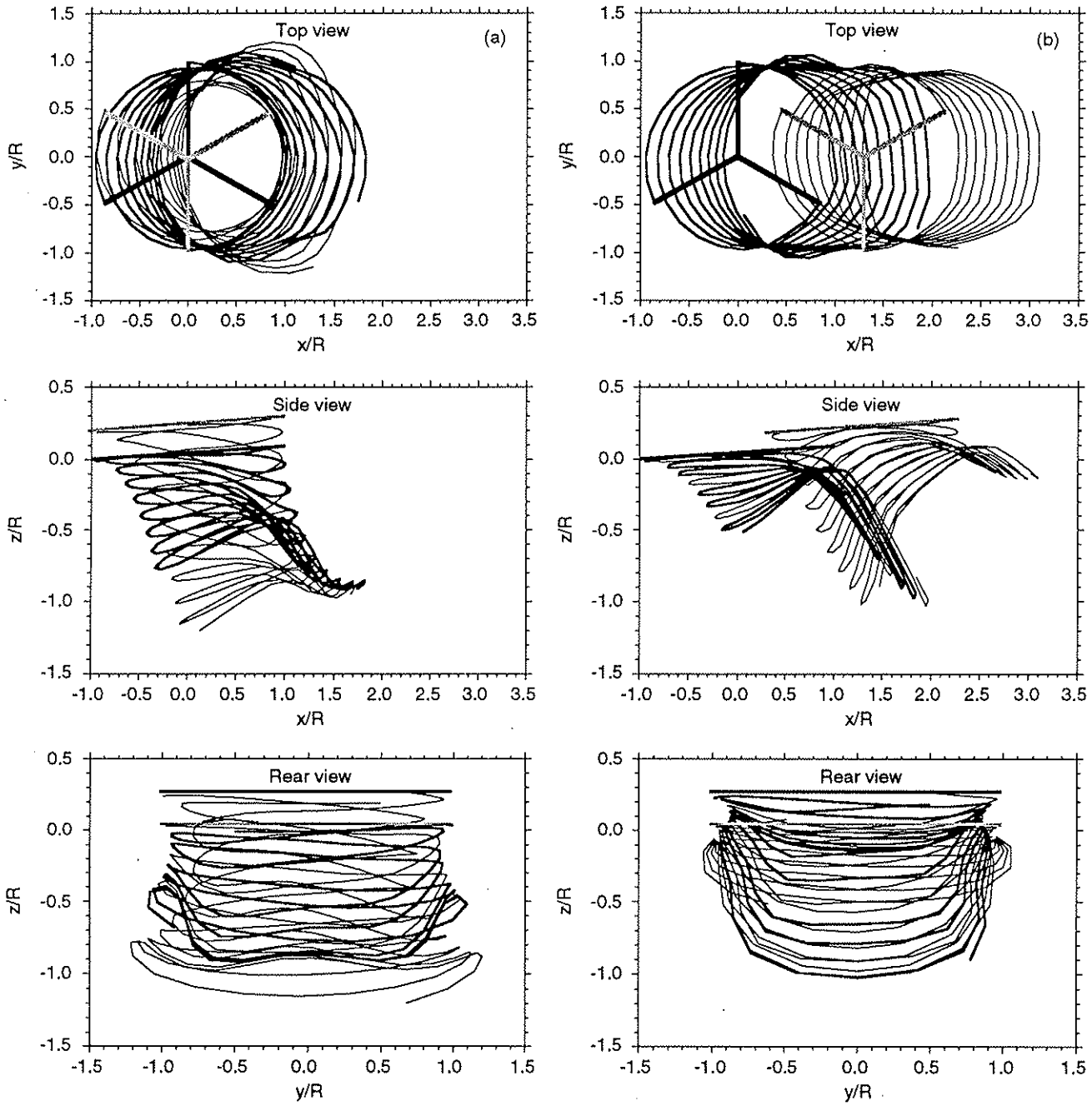

Figure 3: Top, side and rear views of twin rotor configurations, (a) Co-axial, (b) Tandem, 3 turns of far wake, μ=0.05, $\Delta\psi = 15° = \Delta\zeta$, α_{s1} = -3° = α_{s2}

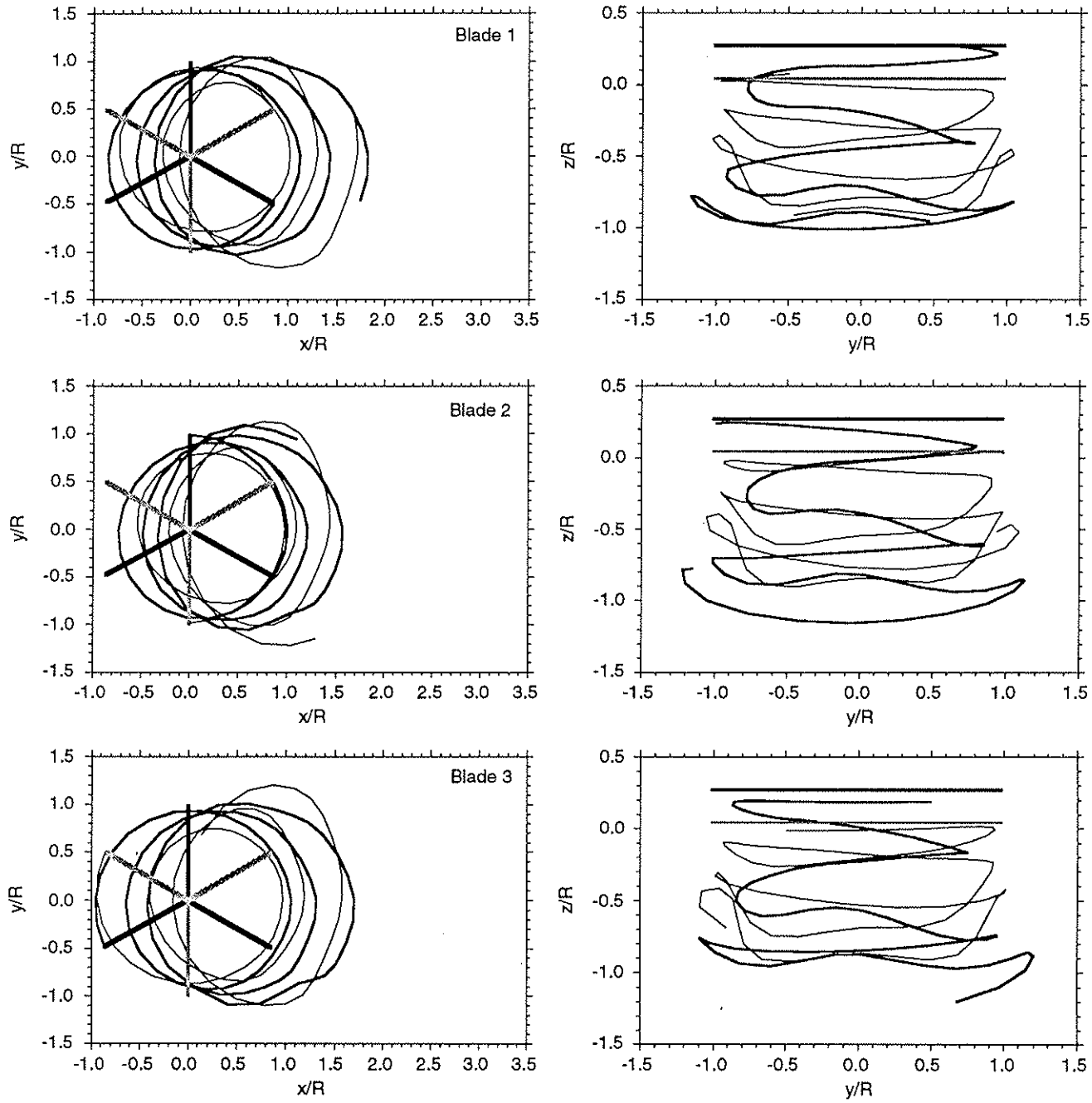

Figure 4: Top and rear views of individual tip vortex trajectories for co-axial rotor, 3 turns of far wake, μ=0.05, $\Delta\psi = 15° = \Delta\zeta$, α_{s1} = -3° = α_{s2}

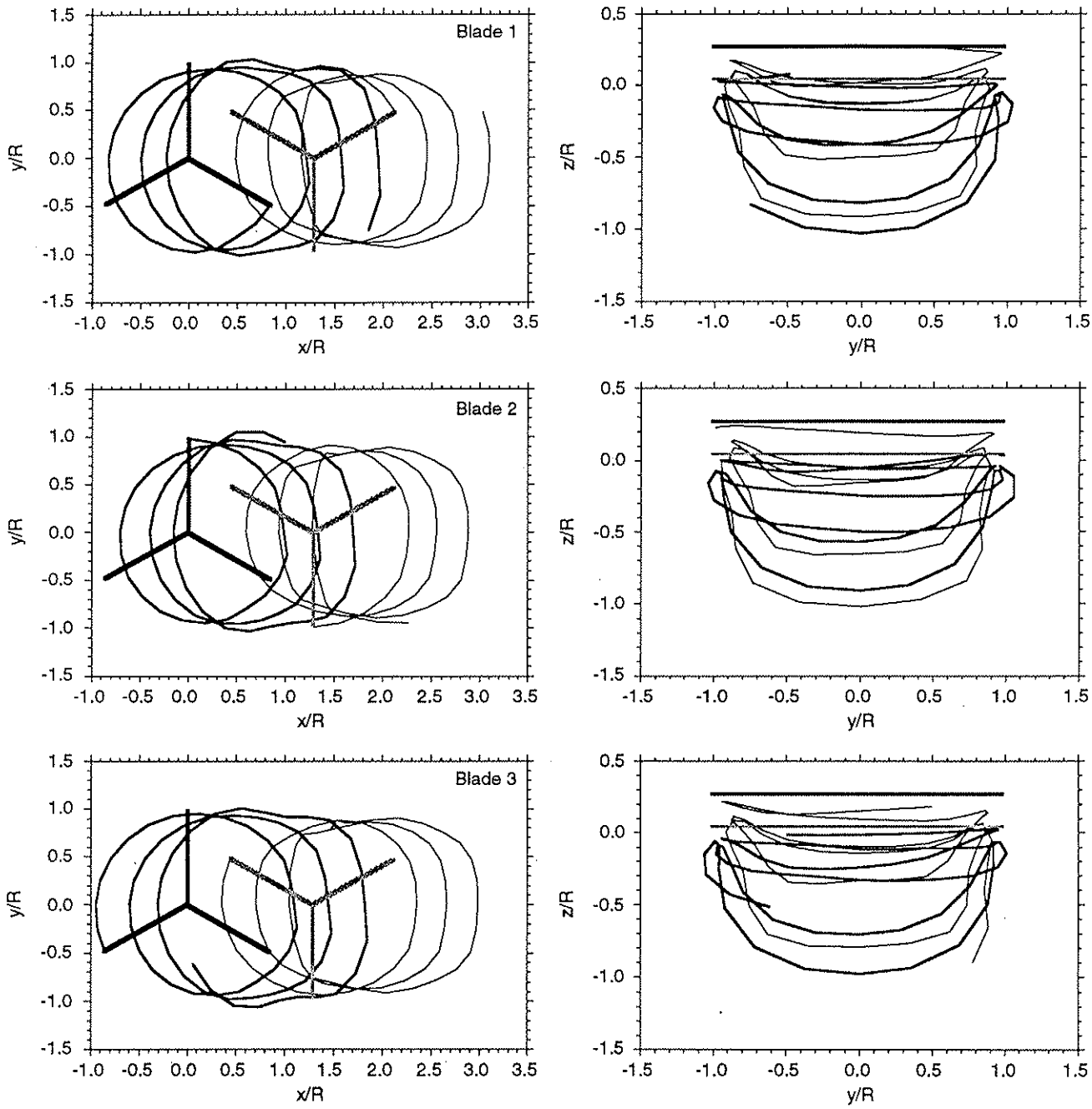

Figure 5: Top and rear views of individual tip vortex trajectories for tandem rotor, 3 turns of far wake, μ=0.05, $\Delta\psi = 15° = \Delta\zeta$, α_{s1} = -3° = α_{s2}

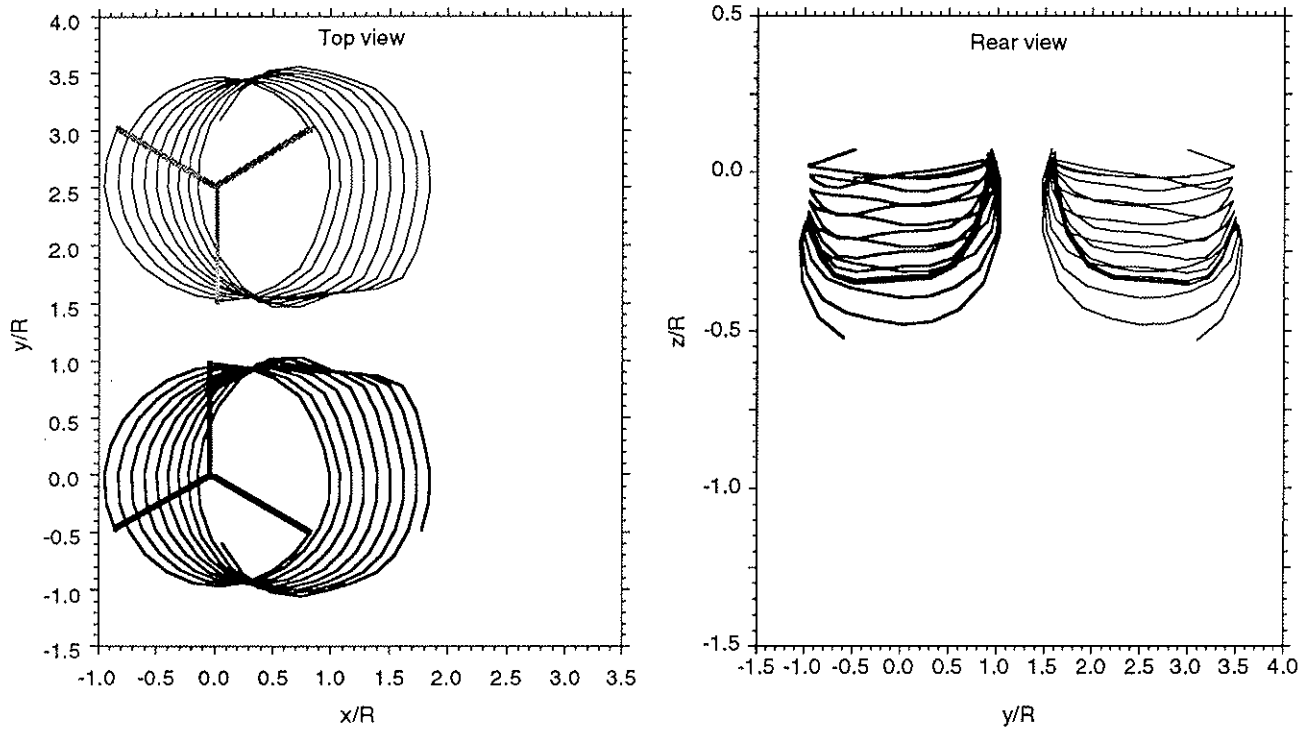

Figure 6: Top and rear views of the side-by-side configuration $\mu = 0.05$, 3 turns of far wake, $\Delta\psi = 15° = \Delta\zeta$, α_{s1} = -3° = α_{s2}

below. The tandem configuration, on the other hand, Fig 3(b) and Fig. 5, shows a greater degree of intermingling between the tip vortices from the two rotors, and this increases with advance ratio. Since the second rotor is above and behind the first rotor, the rear portion of the first rotor wake and the forward region of the second rotor wake undergo the greatest amount of mutually induced distortion.

Lateral distortions to the wake structures are most pronounced for the side-by-side rotors, Fig. 6. As is clearly apparent in the rear view of this configuration, the mutually reinforced upwash due to the two rotors results in a stronger roll-up of the vortices on the advancing sides of the rotor disks. Remember that since the rotor on the left is rotating in a counter-clockwise sense and the one on the right is clock-wise, there is a region of upwash between them, producing tightly rolled up vortex bundles.

Slightly higher advance ratios have also been investigated, all of which are relatively difficult test cases. The predicted converged geometries at μ=0.05, μ=0.075 and μ=0.1 are presented in isometric views in Fig. 7. These results clearly show the distortions to the rotor wake structure due to the mutual interactions between the vortices in the rotor flow-field. The increasing skewness of the wake with increasing advance ratio is also clearly apparent for all three rotor systems. Furthermore, note also that the absence of numerical perturbations in the geometry suggests that the wakes from both rotors have properly converged. For greater clarity, the wakes from the two rotors for the co-axial and tandem rotors at μ=0.1 have been separated, and are shown in Fig. 8. The co-axial rotor clearly shows how the vortices from the upper rotor retain their tubular structure regardless of the start of the roll-up of the far wake downstream of the rotor disks. The tandem rotor wakes on the other hand clearly undergo significant vertical distortions where the two rotor wakes tend to entrain each other vertically.

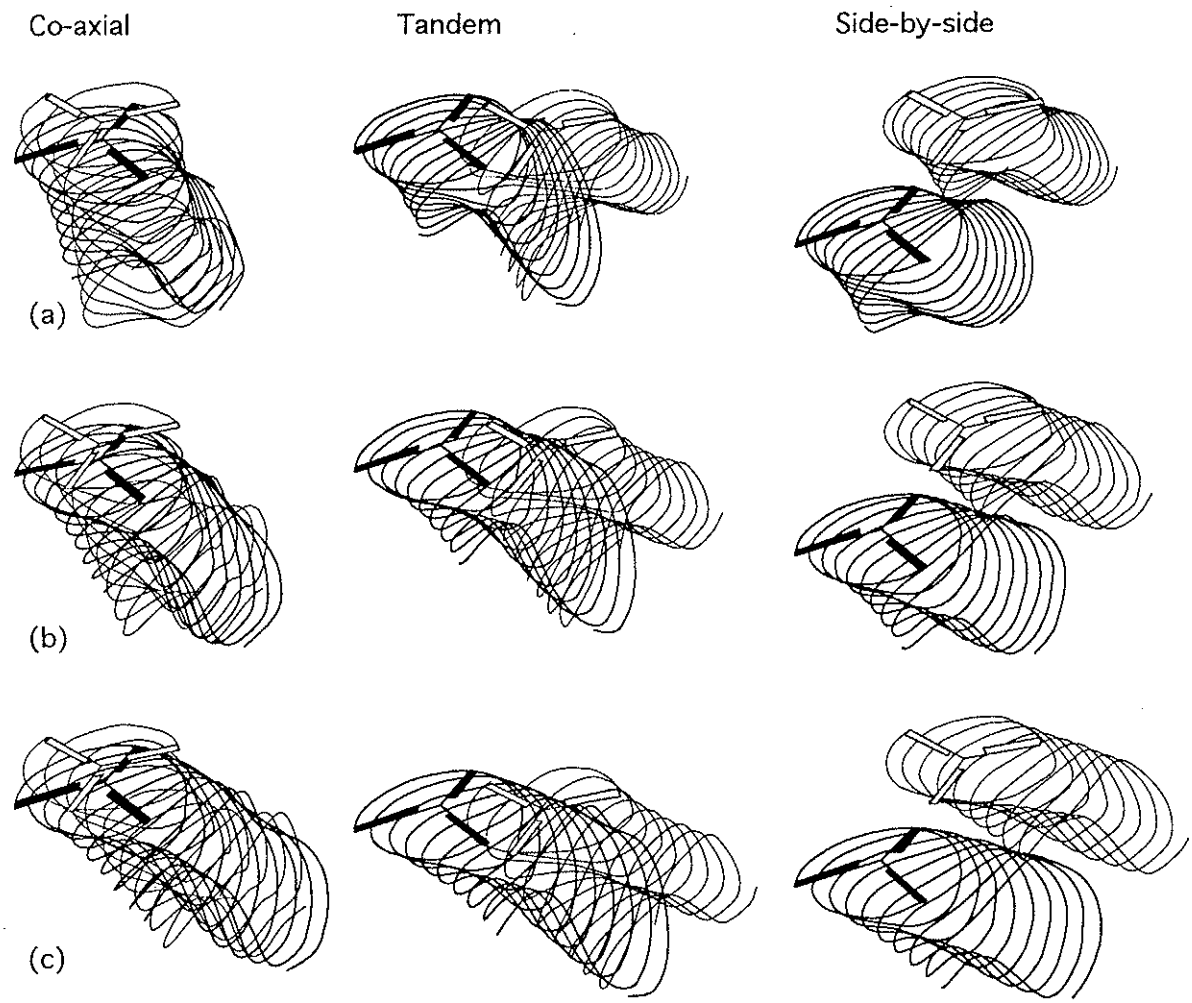

Figure 7: Isometric views of the three twin rotor configurations, (a) $\mu = 0.05$, (b) $\mu = 0.075$ and (c) $\mu = 0.1$, 3 turns of far wake, $\Delta\psi = 15^\circ = \Delta\zeta$, $\alpha_{s1} = 3^\circ = \alpha_{s2}$

Convergence Characteristics

It is necessary to impose a convergence criterion on the PIPC relaxation scheme. In the present work, this has been based on a measure of the L_2 norm (RMS) of the change in the tip vortex geometry locations between two successive wake iterations. An expression for the RMS change can be written in the following form

$$RMS = \frac{1}{j_{max}\, k_{max}} \sqrt{\sum_{\psi:j=1}^{j_{max}} \sum_{\zeta:k=1}^{k_{max}} \left(\vec{r}_{j,k}^{\,n} - \vec{r}_{j,k}^{\,n-1} \right)^2} \tag{10}$$

Wake convergence is reached after the RMS value drops below a certain prescribed threshold between two successive wake iterations. In practice, this RMS change must fall to an order of magnitude of 10^{-4} to ensure that the wake has fully converged. For RMS values of this order of magnitude the wake geometry is known through numerical experimentation to exhibit no appreciable change between successive iterations. Convergence of the wake geometries is important in determining the final solution to the free-wake problem; unfortunately, however, convergence is by no means guaranteed. Indeed it is very strongly dependent on a number of numerical aspects such as finite differencing schemes, integration models, the mathematical modeling of the vortex physics, the number of far wake turns and resolution, as well as the flight condition and blade loadings (which essentially determine the vortex strengths). While the PIPC scheme has been shown to exhibit excellent convergence characteristics for single rotor wakes, from hover through high speed forward

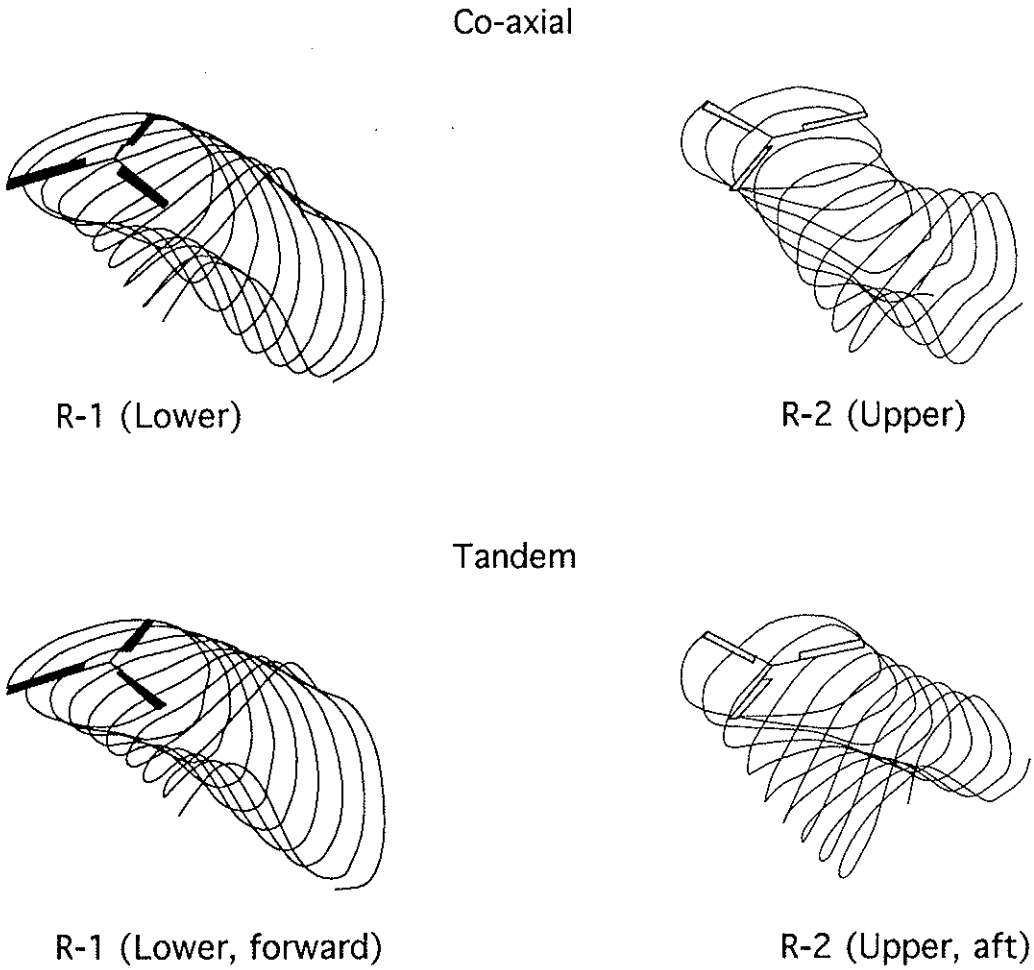

Figure 8: Separated isometric views for the co-axial and tandem rotor configurations at $\mu = 0.1$

flight (Ref. 19) it has not been previously applied to twin rotor systems.

Wake convergence characteristics for the three twin rotor systems are shown in Figs. 9 through 11, respectively. While it has been found that twin rotor systems generally require a greater number of wake iterations until convergence is obtained compared to single rotor wake systems, the convergence rate are actually only marginally slower.

The wake convergence histories for the co-axial rotor wake is shown in Fig. 9 which shows how the rate of convergence for each of the individual rotor wakes increases with increasing advance ratio. In fact, even though there are powerful interactions between the individual wakes, it has been found that co-axial rotors exhibit wake convergence characteristics very similar to that of single (isolated) rotors – see Ref. 20 – in that is the number of iterations for convergence increases slightly with decreasing advance ratio. This is due to the closer proximity of all the individual vortex filaments at low advance ratios, and a somewhat more intense mutual interaction between the vortex filaments. It is also interesting to note that the upper rotor wake converges slightly faster than the outer wake structure, and that this difference is more significant at the higher advance ratios.

The tandem rotor convergence histories on the other hand, show only slight changes with increasing advance ratio – see Fig. 10. For the lower (forward) rotor, there is a slight change in convergence rate with advance ratio, but no distinct trend was observed. For the upper (rear) rotor, the change in convergence rates for the upper rotor is practically insignificant. Again, these results are related to the strengths of the individual tip vortices and their mutual interactions. For the tandem, there is a powerful mutual interaction between the wake vortices.

For the side-by-side rotor system, Fig. 11 shows how similar the convergence histories are for both rotors. This is not an unexpected result, since the symmetry of the side-by-side configuration should result in a mutually equal distortion to both rotor wakes. As the wakes converge, however, a slight difference in the convergence rates is manifest. This difference is possibly due to numerical differences incurred in the wake geometries due to the sequential form of the free-wake iterations, as mentioned previously, which introduces slight differences in the mutual induced velocity field for the two rotors and resulting wake structures. These differences then result in slightly asymmetric

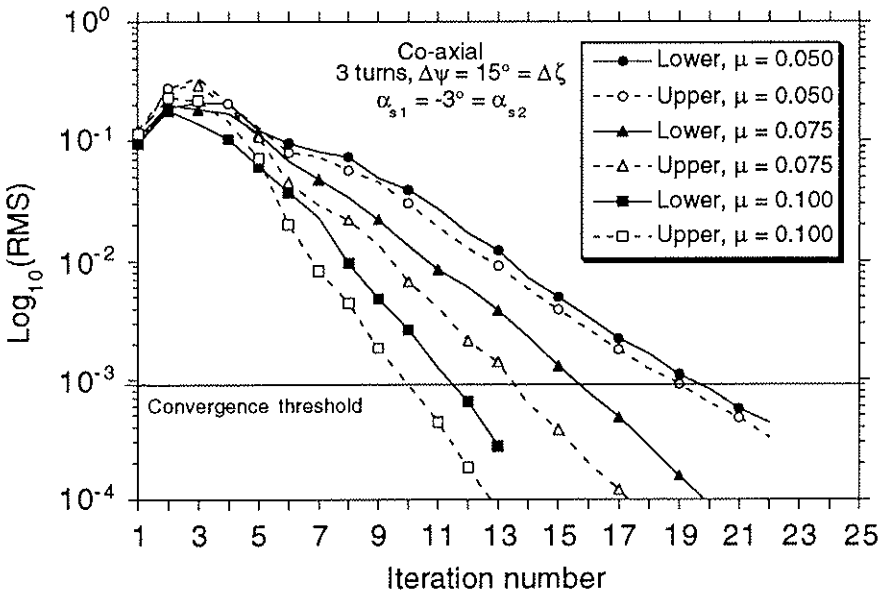

Figure 9: Convergence history for the co-axial rotor configuration

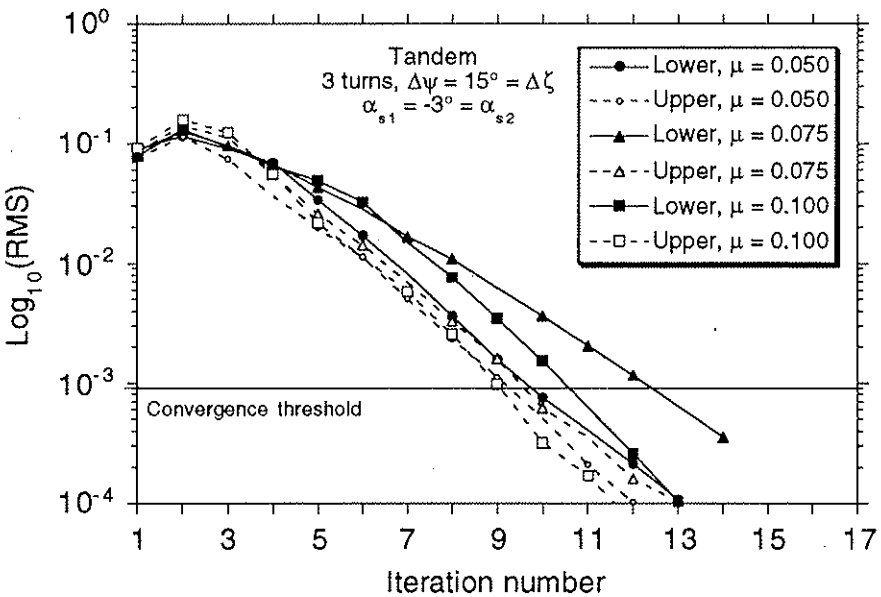

Figure 10: Convergence history for the tandem rotor configuration

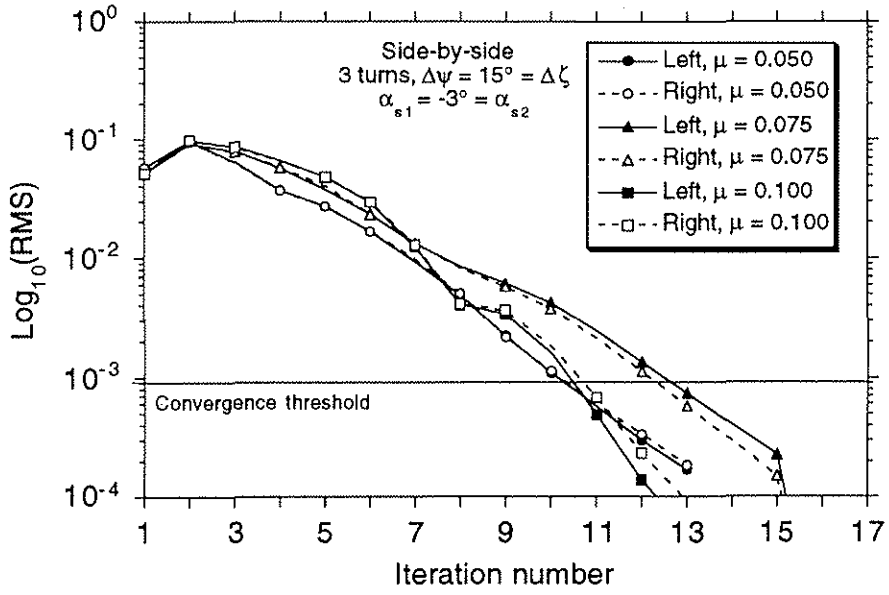

Figure 11: Convergence history for the side-by-side rotor configuration

blade loads, and also result in slightly different trim conditions. As the iterations proceed, these differences apparently grow somewhat, and so the two wakes converge to slightly different solutions. The side-by-side rotors otherwise exhibit convergence characteristics very similar to a single isolated rotors wake (Ref. 20).

It is interesting to further note, however, that the tandem and side-by-side configurations converge significantly faster than the co-axial rotor wake, particularly at lower advance ratios. Also, as mentioned previously, the convergence characteristics are influenced by the angular resolution of the far wake (number of collocation points on the vortex filaments). Initial results however, have shown only a slight decrease in the convergence rates with increasing wake resolution.

4. CONCLUDING REMARKS

A free-wake methodology has been developed and applied to investigate the wake structure from twin rotor systems, namely co-axial, tandem and side-by-side configurations. The basic formulation of the free-wake is based on a pseudo-implicit, predictor-corrector relaxation scheme with five-point central differencing in space, and is identical to that previously developed for single rotors. The method has shown excellent wake convergence characteristics leading to a physically correct distorted wake structure, lending considerable confidence to the current method.

Although results from only three basic twin rotor configurations have been presented here, the current PIPC scheme has also been applied to overlapping side-by-side rotors, and co-axial and tandem systems with various separations and rotor shaft tilts. Results from these tests have been very encouraging and also exhibited very good convergence trends. Higher resolution wakes suitable for rotor acoustic studies have also been investigated with similar results.

While the PIPC scheme has been shown to be robust and well suited for twin rotor systems, no numerical predictive model is complete without validation with experiment. There is some experimental data on co-axial rotor wake geometries in the literature, and while a detailed comparison is outside the scope of the present article, initial results are promising. For the tandem and side-by-side configurations, however, little or no experimental measurements of the wake geometry currently exist.

ACKNOWLEDGEMENTS - This work was supported by the US. Army Research Office under contract DAAH-04-93-G-001. The authors would like to thank Dr. James Baeder for helpful discussions on the numerical aspects of the free-wake problem.

REFERENCES

[1] A. V. Larin, "Vortex Wake Behind a Helicopter," *Aviatsiya i kosmonavtika*, No. 3, pp. 32-33, 1973. Avail. NTIS as translation ADA005479, 1974.

[2] A.V. Larin, "Vortex Formation in Oblique Flow Around a Helicopter Rotor," *Uchenyye Zapiski TSAGI*, Vol. 1, No. 3, pp. 115-122, 1970. Avail. NTIS as translation AD781245, 1974.

[3] Bi, Nai-pei, Leishman, J. G., "Experimental Study of Aerodynamic Interactions between a Rotor and a Fuselage," *Journal of Aircraft*, Vol. 27, No. 9, Sept. 1990.

[4] Crouse, G.L., Leishman, J.G., "Interaction Aerodynamic Effects on Rotor Performance in Hover and Forward Flight," Proceedings of the *48th Annual Forum of the American Helicopter Society*, Washington D.C., June 3-5, 1992.

[5] R.H. Spencer, "Application of Vortex Visualization Test techniques to Rotor Noise Research," *Proceedings of the Annual Forum of the American Helicopter Society*, May 1969.

[6] H. Sternfeld, J.O. Schairer, "Study of Rotor Blade Tip Vortex Geometry for Noise and Airfoil Applications," Boeing Helicopters D8-2464-1A, Dec. 1969.

[7] A. J. Landgrebe, "An Analytical Method for Predicting Rotor Wake Geometry," *Journal of the American Helicopter Society*, Vol. 14, No. 4, Oct. 1969, pp. 20–32.

[8] A.J. Landgrebe, "An Analytical and Experimental Investigation of Helicopter Rotor Performance and Wake Geometry Characteristics," USAAMRDL TR 71-24, June 1971.

[9] J. D. Kocurek and L. F. Berkowitz, "Velocity Coupling — A New Concept for Hover and Axial Flow Wake Analysis and Design," AGARD CP 334, May 1982.

[10] T.A. Egolf, A.J. Landgrebe, "Helicopter Rotor Wake Geometry and its Influence in Forward Flight, Vol. I - Generalized Wake Geometry and Wake Effect on Rotor Airloads and Performance," NASA CR-3726, Oct. 1983.

[11] T.S. Beddoes, "A Wake Model for High Resolution Airloads," *Proceedings of the 2nd International Conference on Basic Rotorcraft Research*, Triangle Park, NC, 1985.

[12] A.F. Lehman, "Model Studies of Helicopter Rotor Patterns," *Proceedings of the 24th Annual Forum of the American Helicopter Society*, May 1968.

[13] A.J. Landgrebe, E.D. Bellinger, "An Investigation of the Quantitative Applicability of Model Helicopter Rotor Wake Patterns Obtained from a Water Tunnel," UARL K910917-23, Dec. 1971.

[14] M.J. Andrew, "Co-axial Rotor Aerodynamics in Hover," *Vertica*, Vol. 5, pp. 163-172, 1981.

[15] T. Nagashima, H. Ouchi, F. Sasaki "Optimum Performance and Load Sharing of Coaxial Rotor in Hover," *Journal of the Japan Society of Aeronautics and Space Sciences*, 1976.

[16] D.R. Clark and A.C. Leiper, "The Free Wake Analysis – A Method for the Prediction of Helicopter Rotor Hovering Performance," *Journal of the American Helicopter Society*, Vol. 15, No. 1, Jan. 1970, pp. 3–11.

[17] S.G. Sadler, "A Method for Predicting Helicopter Wake Geometry, Wake-Induced Flow and Wake Effects on Blade Airloads," Presented at the 27th Annual National Forum of the American Helicopter Society, May 1971.

[18] W.O. Miller and D.B. Bliss, "Direct Periodic Solutions of Rotor Free Wake Calculations by Inversion of a Linear Periodic System," In *Proceedings of the 46th Annual Forum of the American Helicopter Society*, Washington, DC, May 1990, pp. 757–769.

[19] A. Bagai and J.G. Leishman, "Rotor Free-Wake Modeling using a Relaxation Technique – Including Comparisons with Experimental Data," Presented at the 50th Annual National Forum of the American Helicopter Society, Washington, D.C.,May 11-13 1994.

[20] A. Bagai and J.G. Leishman, "Rotor Free-Wake Modeling using a Pseudo-Implicit Relaxation Algorithm," Presented at the 12th AIAA Applied Aerodynamics Conference, Colorado Springs, CO, June 20-23 1994.

[21] V.J. Rossow, "On the Inviscid Rolled-Up Structure of Lift Generated Vortices," *J. of Aircraft*, Vol. 10, No. 11, Nov. 1973, pp. 647-650.

[22] A. Bagai and J.G. Leishman, "Flow Visualization of Compressible Vortex Structures using Density Gradient Techniques," *Experiments in Fluids*, Vol. 15, 1993, pp. 431-442.

[23] Sir Horace Lamb, *Hydrodynamics*, 6th edition, Cambridge University Press, 1932, pp. 592-593, 668-669.

[24] D.A. Anderson, J.C. Tannehill and R.H. Pletcher, *Computational Fluid Mechanics and Heat Transfer*, Hemisphere, Cambridge, 1984.

[25] Akimov, A. I., Butov, V. P., Bourtsev, B. N., Selemenev, S. V., "Flight Investigation of Coaxial Rotor Tip Vortex Structure," Presented at the 50th. Annual Forum of the *American Helicopter Society*, Washington, D.C., May 1994.